PHYSICAL REVIEW D **93,** 123015 (2016)

Black hole spin influence on accretion disk neutrino detection

O. L. Caballero* and T. Zielinski
Department of Physics, University of Guelph, Guelph, Ontario N1G 2W1, Canada

G. C. McLaughlin
Department of Physics, North Carolina State University, Raleigh, North Carolina 27695, USA

R. Surman
Department of Physics, University of Notre Dame, Notre Dame, Indiana 46556, USA
(Received 27 October 2015; published 22 June 2016)

Neutrinos are copiously emitted from neutrino-cooled black hole accretion disks playing a fundamental role in their evolution, as well as in the production of gamma ray bursts and r-process nucleosynthesis. The black hole generates a strong gravitational field able to change the properties of the emerging neutrinos. We study the influence of the black hole spin on the structure of the neutrino surfaces, neutrino luminosities, average neutrino energies, and event counts at SuperK. We consider several disk models and provide estimates that cover different black hole efficiency scenarios. We discuss the influence of the detector's inclination with respect to the axis of the torus on neutrino properties. We find that tori around spinning black holes have larger luminosities, energies, and rates compared to tori around static black holes and that the inclination of the observer causes a reduction in the luminosities and detection rates but an increase in the average energies.

DOI: 10.1103/PhysRevD.93.123015

I. INTRODUCTION

The physics of stellar phenomena such as gravitational radiation, the synthesis of heavy elements, and short gamma ray bursts is closely tied to the emission of neutrinos from black hole (BH) accretion disks (AD). These systems can be one possible outcome from BH-neutron star (NS) and NS-NS mergers [1–4], or rapidly rotating stars (collapsars). Although these events are rare (estimated rates are $10^{-6} - 10^{-3}$/year per Milky Way equivalent galaxy (MWEG) for NS-NS mergers, and $10^{-8} - 3 \times 10^{-5}$/year per MWEG for BH-NS mergers [5]), the importance of neutrinos in these phenomena motivates their further study. In relation to the synthesis of elements, given the neutron richness of their progenitors, BH-AD are proposed as good candidates for r-process nucleosynthesis [6–9], where neutrinos play the crucial role of setting the initial electron fraction of the outflowing matter [8,10]. On the other hand, because of the vast amount of neutrinos emitted, neutrino annhilitation above the BH could provide the conditions needed to trigger gamma ray bursts [11–15]. Equally interesting, and in correlation with multimesenger signals (see, e.g., [16,17]), is the possibility of neutrino detection from ADs in future and current facilities as has been discussed in several works [18–20].

Fully three-dimensional general relativistic simulations are needed to study the implications of the spacetime metric and of neutrino cooling on the evolution of BH-NS or NS-NS mergers [21–26]. Such simulations have shown that the evolution of the binary mergers depends on the initial binary parameters [22]. In particular, in BH-NS mergers, the BH spin and its alignment characterize the accretion onto the BH [27,28]. These simulations offer an important benchmark for predictions of neutrino energies and luminosities at infinity. They are, however, computationally demanding, making simpler models and postprocessing good alternatives for further studies of neutrino properties.

Much effort has been devoted to studying BH-AD in the Kerr metric (suitable for spinning BHs) and in the Schwarzschild metric (adequate for nonspinning BHs). Some works have studied the structure of neutrino cooled disks accreting into rotating BHs, [12,29] and find higher neutrino fluxes than those obtained from their nonrotating counterparts. Other studies focus on the neutrino annihilation rates and find that the deposition energy from neutrino-antineutrino annihilation is larger for spinning BHs [30–32]. Harikae *et al.* [33] also found considerable changes in the deposition rates when general relativistic effects were considered for neutrinos emitted in a long-term collapsar simulation. However, the dependence of observable properties, such as neutrino energies and event counts, among others, on BH spin has remained unexplored.

Neutrinos in the free streaming regime, i.e., once they have decoupled from the disk matter, can reach an observation (or absorption) point. The neutrino properties, e.g., fluxes, energies, and luminosities observed at the point of emission, will be different from the ones registered by an

*lcaballe@umail.iu.edu

 © 2016 American Physical Society

observer positioned anywhere else. The observed quantities change due to neutrino oscillations [34,35], neutrino interactions, and the gravitational field of the BH. For the latter, the consideration of the three-dimensional geometry of the source is of particular importance, as the relativistic effects (bending of neutrino trajectories and energy shifts) depend on the spacetime curvature. In previous works [36,37], we have studied the influence of gravity on the emission of neutrinos and the production of heavy elements in outflows emerging from BH-AD via a postprocessing of merger simulations and following neutrino trajectories in strong gravity.

Here we extend our study of the neutrino properties by considering the influence of the BH spin and the observer's location. We gain further understanding on the structure of the neutrino surface and its correlation to the BH rotation. We provide estimates of electron antineutrino detection rates, counts and signal duration at SuperK [38] for a variety of AD models. We also discuss angular dependencies of neutrino properties: as the polar inclination of the observer changes, the bending of the neutrino trajectories and energy shifts will be affected. If the gravitational field is strong the curved trajectories allow detection of neutrinos emitted from regions of the neutrino spheres that would be inaccessible otherwise. In Sec. II we discuss the models considered, in Sec. III we study the influence of the BH spin on the structure of the neutrino surfaces, in Sec. IV we show our results for an observer at infinity, and in Sec. V we consider a distant observer at different inclinations. Finally, we motivate further work and conclude in Sec. VI.

II. DISK MODELS

Due to the expensive computational cost of fully relativistic three-dimensional simulations of collapsars and binary mergers, it is worth trying out other approaches to gain physical insight. In this paper we use two different disk models. The first one describes a fully general relativistic steady state disk as in [29]. The second one is a two dimensional time-dependent hydrodynamical simulation of a torus with a pseudorelativistic potential [39].

In the first case, we extend to three dimensions the one-dimensional model from Chen and Belobodorov [29], by estimating the vertical structure using a simple hydrostatic model that assumes that the gas forming the disk is at equilibrium under the gas and radiation pressure. Furthermore, we assume axisymmetry. The model is hydrodynamical and uses the Kerr metric to account for two values of the BH spin $a = Jc/GM^2$ (J is the total angular momentum and M the BH mass). We label these models according to the BH spin: "C0" for $a = 0$ and "Ca" for $a = 0.95$. The mass of the BH is $3M_\odot$, the accretion rate $\dot{M}$ is constant, and the viscosity parameter is $\alpha = 0.1$.

In the second model, from Just *et al.* [39], the simulation is set up to be the equilibrium configuration of a constant angular momentum axisymmetric torus that emulates the final stages of compact binary mergers. The BH mass is $3M_\odot$, the alpha viscosity is $\alpha = 0.02$, and the BH spins are $a = 0$ and $a = 0.8$. We refer to these tori as J0 and Ja, respectively. The simulation is Newtonian and the gravitational effects of the BH are introduced via a modified Newtonian potential which is an extension of the Paczynski-Wiita potential [40] to rotating BHs [41]. This reproduces the radius of the innermost stable circular orbit in the Kerr metric. The structure of the torus evolves in time. To study the effects of the BH spin on the neutrino surfaces, we use a $t = 20$ ms snapshot, when presumably the neutrino fluxes are the largest [36,42].

III. NEUTRINO SURFACES

The neutrino surfaces, analogous to the neutrino spheres of a protoneutron star (PNS) from core collapse supernovae, are defined by the points above the equatorial plane where neutrinos decouple from the accretion torus. This happens when the neutrino optical depth $\tau = 2/3$. Assuming z as the direction of neutrino progration, then τ, in terms of the opacity κ_ν and the mean free path l_ν, is given by

$$\tau_\nu(x,y) = \int_{z_\nu}^{\infty} \kappa_\nu(z')dz' = \int_{z_\nu}^{\infty} \frac{1}{l_\nu(x,y,z')}\,dz'. \quad (1)$$

The surface corresponds to the triplet (x, y, z_ν) such that the lower limit z_ν leads to the value $\tau = 2/3$.

The mean free path l_ν involves all relevant scattering processes that neutrinos undergo as they diffuse through the torus. As matter is accreted into the BH, it becomes hotter and nuclei dissociate. Therefore, we consider neutrino scattering from protons, neutrons, and electrons. We take into account absorption through the charged current processes,

$$\nu_e + n \rightarrow p + e^-, \quad (2)$$

$$\bar{\nu}_e + p \rightarrow e^+ + n, \quad (3)$$

and the neutral current processes $\nu + n \rightarrow \nu + n$ and $\nu + p \rightarrow \nu + p$. We also consider elastic scattering from electrons and neutrino-antineutrino annihilation. The charged current reactions affect only electron (anti)neutrinos while the other processes affect all neutrino flavors. As tau and muon neutrinos scatter through the same processes, we label these flavors as ν_x. We find proton and neutron number densities assuming charge neutrality $Y_e = Y_p$, and the electron number density assuming equilibrium of thermal electrons and positrons with radiation.

Our calculation of the mean free path is then given by the sum

$$l_\nu(x,y,z) = \frac{1}{\sum_k n_k \langle \sigma_k(E_\nu)\rangle}, \tag{4}$$

where n_k is the number density of a particular target with cross sections σ_k. Details on the cross sections of the above reactions can be found in Ref. [20]. $\langle \sigma_k(E_\nu)\rangle$ is the thermally averaged cross sections that assumes a Fermi-Dirac distribution for the neutrinos with a temperature equal to the local torus temperature and zero chemical potential,

$$\langle \sigma_k(E_\nu)\rangle = \frac{\int_0^\infty \sigma_k(E_\nu)\phi(E_\nu)dE_\nu}{\int_0^\infty \phi(E_\nu)dE_\nu}, \tag{5}$$

with $\phi(E_\nu)$ the neutrino flux written in terms of the Fermi-Dirac distribution f_{FD},

$$\phi(E_\nu) = \frac{c}{2\pi^2(\hbar c)^3}(E_\nu)^2 f_{FD}. \tag{6}$$

This procedure removes the energy dependence of the neutrino surface, as our results have been properly energy weighted. Note, however, that the scattering neutrino surfaces differ from the effective neutrino surfaces (see, e.g., [43]) with the difference being larger for tau and muon neutrinos.

Figure 1 shows a quarter of the electron neutrino and electron antineutrino surfaces corresponding to the Ca model ($a = 0.95$) and $\dot{M} = 5M_\odot/\mathrm{s}$. The color scale represents the neutrino temperatures. The hotter neutrinos (yellow) are emitted closer to the BH. These will have the biggest contribution to the net neutrino fluxes. Tau/muon neutrino surfaces, not shown for clarity, are the hottest ($T_{\nu_x} \approx 10.5$ MeV), followed by the electron antineutrino surfaces ($T_{\bar{\nu}_e} \approx 9$ MeV). The coolest are the electron neutrino surfaces which are the farthest from the BH ($T_{\nu_e} \approx 8$ MeV). This is similar to the flavor hierarchy found in the PNS neutrino spheres, and can be understood in terms of the reactions Eqs. (1) and (2). Since the torus is abundant in neutrons, electron neutrino absorption on them [Eq. (2)] will have a more substantial effect on the mean free path than electron antineutrino absorption on protons [Eq. (3)], causing electron neutrinos to decouple at the lowest temperatures. ν_x lack these charged current processes and decouple closest to the BH where the temperatures are higher.

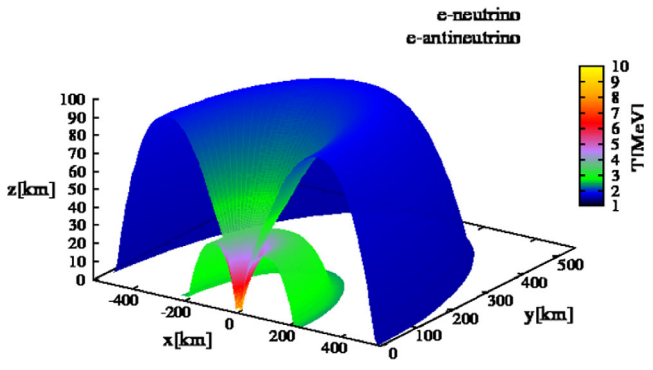

FIG. 1. Electron neutrino surface (outer) and electron antineutrino surface (inner) based on the Ca torus model with a BH spin $a = 0.95$, $\dot{M} = 5M_\odot/\mathrm{s}$ and $3M_\odot$ BH [29]. The color scale shows the corresponding neutrino temperatures.

The geometry and temperatures of the neutrino surfaces for these tori are, however, different from those of a PNS. In the torus, near the BH, due to the gravitational potential, the accreted matter forms a funnel with lower densities. Closer to the BH, there is an increment of the temperature, as matter radiates energy when falling to the BH. The emitted neutrinos move through this less dense medium for a shorter time, producing higher temperatures compared to a PNS. In the PNS, neutrinos diffuse through a denser medium, compared to a BH-AD, and decouple at lower temperatures ($T_{\nu_e} \approx 2.6$, $T_{\bar{\nu}_e} \approx 4$, and $T_{\nu_x} \approx 5$ MeV) [19].

Figure 2 shows a transversal cut of the electron antineutrino surfaces for the two models used here: Chen-Beloborodov with $\dot{M} = 5M_\odot/\mathrm{s}$ (dotted lines) and Just *et al.* (solid lines). For each model, we find the electron antineutrino surfaces for two different spin parameters, $a = 0$ and $a = 0.95$, corresponding to the C0 and Ca models, respectively, and $a = 0(0.8)$ for the J0(Ja) models. In both sets of models, the taller surfaces correspond to the higher spin values. The color scale represents the temperature $T_{\bar{\nu}_e}$ at the decoupling points. These are higher for spinning BH regardless of the disk model. For the Ca model, $T_{\bar{\nu}_e}$ are as high as 9 MeV, while they are around 4.5 MeV for the C0 case. Similarly, for the Ja model $T_{\bar{\nu}_e}$,

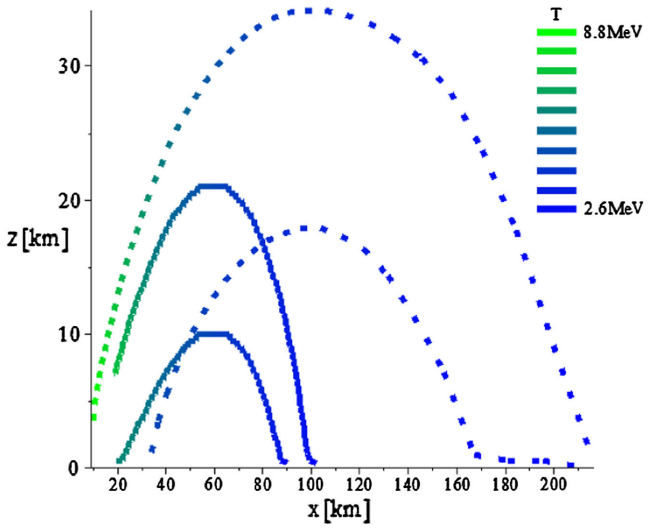

FIG. 2. Comparison of electron antineutrino surfaces for different BH spins and different disk models. Dotted lines are for the models C0 ($a = 0$) and Ca ($a = 0.95$), while solid lines correspond to J0 ($a = 0$) and Ja ($a = 0.8$). The taller lines for each model correspond to the higher spins.

the maximum is 7 MeV, while for J0 the highest value is around 6 MeV. The BH spin also affects the extension of the disk; the higher the spin the larger the neutrino surface of the torus. This, as we explain later, impacts the neutrino luminosities and detection rates. Note, furthermore, that the α viscosity parameter of the two models is very different: 0.02 for the dynamical model and 0.1 for the steady state one. This also contributes, through increasing angular momentum transport, to the differences seen in the structure of the neutrino surfaces.

Hotter neutrino surfaces for larger spins a are a consequence of the spacetime geometry. Matter rotating around a BH will release energy before plunging into it. The radius of the marginally stable circular orbit r_I, also known as the innermost stable circular orbit or ISCO, is the smallest circle along which free particles may stably orbit around a BH. The binding energy that can be released increases as r_I decreases, and r_I decreases with the increment of the BH spin [44]. When the angular momentum per unit mass exceeds r_I centrifugal forces will be significant and the matter will circulate around the BH. The extra angular momentum will be carried away by viscous stress. The viscous heating can then be converted to neutrino luminosity. The extension of the neutrino surfaces is also linked to spacetime geometry. In Kerr BHs matter is hotter and denser when compared to Schwarzschild BHs. Neutrinos scatter in this denser medium taking, therefore, a larger distance to decouple which is reflected in larger neutrino surfaces.

IV. DISTANT OBSERVATION

Using our results for the neutrino surfaces, and following a similar methodology as in Refs. [20,25], we can estimate the number of neutrinos emitted per sec f^e, the emitted luminosities L^e_ν, and average energies $\langle E^e_\nu \rangle$ as

$$f^e = \frac{dN}{dt^e} = \int dA^e dE^e \phi^{\rm eff}(E^e), \tag{7}$$

$$L^e_\nu = \frac{dE^e}{dt^e} = \int dA^e dE^e E^e \phi^{\rm eff}(E^e), \tag{8}$$

and

$$\langle E^e_\nu \rangle = \frac{dE^e/dt^e}{f^e}, \tag{9}$$

where the effective flux, i.e., the number of neutrinos emitted per unit energy, per unit area, per second, is

$$\phi^{\rm eff}(E^e) = \frac{1}{4\pi}\int d\Omega^e \times \phi(E^e), \tag{10}$$

and $\phi(E^e)$ is the Fermi-Dirac flux [Eq. (6)]. In the equations above, the integral over dA^e corresponds to an integral over the neutrino surface. Assuming isotropic emission will reduce the integral over $d\Omega^e$ to 4π. The transformation of these quantities to an observer located at infinity can be done by using the invariance of phase-space density [25,37],

$$\frac{1}{c^2}\frac{dN}{d^3x_o d^3p_o} = \frac{1}{c^2}\frac{dN}{d^3x_e d^3p_e}, \tag{11}$$

with the subindex o denoting observed quantities. The relation between the observed E^o and emitted E^e energies is $E^e = (1+z)E^o$ where $(1+z)$ is the redshift. To a distant observer the distances appear stretched roughly by a factor of $(1+z)$, changing the areas accordingly. Putting this together, we have

$$\frac{dN}{dt^o} = \int \frac{1}{(1+z)}\phi(E^e) dE^e dA^e, \tag{12}$$

$$\frac{dE^o}{dt^o} = \int \frac{1}{(1+z)^2}\phi(E^e) E^e dE^e dA^e, \tag{13}$$

and

$$\langle E^o_\nu \rangle = \frac{dE^o/dt^o}{f^o}. \tag{14}$$

The number of neutrinos reaching a detector per second R is given by

$$R = N_T \int_{E_{th}}^{\infty} \phi^{\rm eff}(E^o)\sigma(E^o) dE^o, \tag{15}$$

where N_T is the number of targets in the detector, E^o are the neutrino energies registered, and $\sigma(E^o)$ is the detector's neutrino cross section. The effective flux $\phi^{\rm eff}(E^o)$ reaching the detector is

$$\phi^{\rm eff}(E^o) = \frac{1}{4\pi}\int d\Omega^o \times \phi(E^o_\nu), \tag{16}$$

where $d\Omega^o$ is the solid angle that the torus subtends as seen by an observer at the detection point, i.e., $d\Omega_o = \sin\xi d\xi d\alpha$, where ξ, α are spherical coordinates in the observer's sky.

We are interested in a distant observer. For this situation, the effective fluxes [Eq. (16)] will be strongly influenced by the energy shifts, while the effects of bending of trajectories, reflected in $d\Omega^o$, are smaller. We calculate the energy shifts in the Kerr metric. For the solid angle, we follow the null geodesics that travel away from the neutrino surfaces in the Schwarzschild metric, in order to ease the calculation without compromising our conclusions. Note that if we were interested in an observer that was closer to the BH, a calculation in the Kerr metric would be optimal, as null geodesics in the Kerr metric would lead to larger torus areas, seen by the observer. For a closer observer, estimates of the apparent areas in the Schwarzschild metric would be

an underestimate as compared with those obtained in the full Kerr metric.

For an observer located at infinity, and in the Schwarzschild metric, it suffices to estimate the effect of bending of trajectories by calculating $d\Omega^o = bdbd\alpha/r_o^2$, where b, the neutrino's impact parameter, is

$$b = \frac{r_+}{\sqrt{1 - r_s/r_+}}, \tag{17}$$

r_s is the Schwarzschild radius, and r_+ is the closest distance of the neutrino trajectory to the BH. For a trajectory that goes to infinity, r_+ equals the emission points on the neutrino surface r_e.

On the other hand, the redshift in the Kerr metric depends on the BH spin a, the observer and emitter positions, and their relative velocities (see [37]). For the latter, we assume that the emitter and observer are in Keplerian rotation such that their angular velocities are given by

$$\Omega_{o(e)} = \frac{M^{1/2}}{r_{o(e)}^{3/2} + aM^{1/2}}, \tag{18}$$

with $r_{o(e)}$ the observer(emitter) distance to the BH.

We estimate the number of neutrinos per second that could be detected in SuperK assuming 32 ktons of fiducial volume, with a threshold energy $E_{th} = 5$ MeV [38]. Here the cross section in Eq. (15) corresponds to captures of electron antineutrinos on protons [20]. We also assume that the torus is at 10 kpc from Earth and that we observe it on the z axis, above its equatorial plane. Table I shows the detection rates R observed in SuperK, the observed electron (anti)neutrino luminosities at infinity L^o, and the corresponding observed average energies for the C and J models. Comparing results between the same simulation approach (C0 with Ca, and J0 with Ja) we see that these observables are larger for the higher BH spin, a consequence of the conversion of the extra rotational energy into thermal energy. It is interesting to note that a PNS would produce about 1000 counts/s in SuperK and has a neutrino luminosity of 10^{52} ergs/s [19]. The tori studied here lead to detection rates greater by at least a factor of 10, and luminosities higher by at least 1 order of magnitude, with the difference coming from the hotter neutrino surfaces as discussed in Sec. III.

TABLE I. Observed detection rates R (at 10 kpc in SuperK), electron (anti)neutrino luminosities, and energies for the different accretion tori studied here. In all the models, the BH mass is $3M_\odot$.

	a	R (sec^{-1})	$L^o_{\bar{\nu}_e}$(ergs/s) ($\times 10^{53}$)	$L^o_{\nu_e}$(ergs/s) ($\times 10^{53}$)	$E^o_{\bar{\nu}_e}$ (MeV)	$E^o_{\nu_e}$ (MeV)
J0	0	15000	2.7	1.9	12.7	10.3
C0	0	23900	4.8	4.7	10.3	6.4
Ja	0.8	23600	3.7	2.4	13.4	11
Ca	0.95	58400	9.8	6.8	11.8	7.3

A full comparison of the microphysics of the two models studied here (Chen-Belobodorov vs Just *et al.*) is not the goal of this study. However, we address the differences between the results found in Table I. Although the luminosities are larger for the C0 vs the J0 models, the neutrino energies are lower. The same behavior is observed between the Ca and Ja tori. The differences can be understood in terms of the dependency of the neutrino temperatures with distance to the BH, and the extension of the neutrino surfaces. Close to the BH, where most neutrinos are emitted, the temperatures of C0 and J0 models are similar ~5 MeV (as is also the case for Ca and Ja where T is around tens of MeV). However, the surfaces are much larger for the Chen-Belobodorov models when compared to the Just *et al.* ones. This leads to larger luminosities for C0(Ca) despite the higher temperatures of J0(Ja). Finally, neutrinos emitted farther from the BH contribute to the spectra with lower energies explaining the smaller average energies found for C0(Ca) compared to J0(Ja).

A broader picture of the accretion tori can be achieved by placing our postprocessed results in context with those coming directly from fully relativistic simulations. Recent simulations of the long-term evolution of BH-NS mergers with an initial BH spin $a = 0.9$ and mass ratio of 4 showed the formation of a thick disk of $0.3M_\odot$ and an accretion rate of $\sim 2M_\odot$/s [23]. The total initial neutrino luminosity was found to be around 10^{54} erg/s, dropping to 2×10^{53} erg/s 50 ms later. The neutrino energies, averaged over time, are 12 and 15 MeV for electron neutrinos and antineutrinos, respectively, decreasing at a rate of 1 MeV per 10 ms. These are about 1 MeV larger compared to our spinning BH results of 11 and 13.4 MeV (Ja model) and larger by about 5 and 3 MeV for electron neutrinos and antineutrinos, respectively, for the Ca model. Note that in Ref. [23] neutrino cooling followed a leakage scheme which neglects neutrino absorption. With an improved neutrino cooling scheme that uses an energy-integrated version of the moment formalism F, Foucart *et al.* [21] studied the postmerger evolution of a BH-NS binary, focusing on the stage between disk formation and an achievement of a quasiequilibrum phase. Their merger results in a disk of $0.1M_\odot$ and a BH of $8M_\odot$ with spin 0.87. In this case the luminosities are around $5\text{–}8 \times 10^{52}$ erg/s for electron neutrinos (the leakage scheme predicted luminosities 30% larger), 5×10^{53} erg/s for electron antineutrinos, while the leakage scheme led to estimated energies of 11–13 MeV for electron neutrinos and 14–15 MeV for antineutrinos.

Our results for neutrino luminosities and energies for the spinning models in Table I (in particular for the Ja model), are similar to those coming directly from the cited

simulations despite the fact that the initial conditions are different as well as are the neutrino and gravity treatments. This comparison is useful to roughly check our results and shows that our ray-tracing technique is a reasonable tool for predicting neutrino related quantities via postprocessing studies.

A. Steady accretion tori counts at SuperK

To estimate the total number of counts at SuperK, we multiply the rates [obtained as Eq. (15)] by the duration of the signal. This time can be calculated as the ratio of the energy emitted in the form of neutrinos E_ν^B to the total neutrino luminosity $\Delta t = E_\nu^B/L_\nu$. On the other hand, E_ν^B depends on the efficiency of converting gravitational energy to neutrino energy $\varepsilon = E_\nu^B/E_G$, and so $\Delta t = \varepsilon E_G/L_\nu$. The gravitational energy is the rest mass energy $E_G = M_T c^2$ with M_T the torus mass. We estimate the total number of counts for a collection of fully relativistic steady state tori, similar to the C models above, with different accretion rates. For these models, the viscosity parameter is $\alpha = 0.1$, the BH mass is $3M_\odot$, and the BH spin takes the values $a = 0$ or $a = 0.95$. We estimate ε in two ways. For the first, we assume radial accretion, where $\varepsilon = L_\nu/\dot{M}c^2$ and then $\Delta t = M_T/\dot{M}$. The second estimate accounts for the fact that the accreted matter carries angular momentum and, therefore, the efficiency depends on the BH spin. Then the efficiency ε is $1 - \tilde{E}$ with

$$a = -\frac{4\sqrt{2}(1-\tilde{E}^2)^{1/2} - 2\tilde{E}}{3\sqrt{3}(1-\tilde{E}^2)}, \tag{19}$$

and corresponds to the amount of energy radiated by matter reaching the BH through a series of almost circular orbits. $1 - \tilde{E}$ is the maximum of binding energy at the marginally stable circular orbit which has a radius r_I. Thus, for a BH of $3M_\odot$ with a spin $a = 0$, we find $r_I = 26.49$ km and an efficiency $\varepsilon = 0.057$. For the spinning BH with $a = 0.95$, the efficiency is $\varepsilon = 0.19$ while $r_I = 8.91$ km. These values are replaced in $\Delta t = \varepsilon M_T c^2/L_\nu$. Additionally, we take into account the time dilation occurring in the vicinity of the BH and our time interval as seen at Earth is $\Delta t^o = \Delta t(1+z)$, where this redshift is an estimate taken from the overall redshift between the average observed and emitted neutrino energies. Our results predict signals lasting 0.14 to 0.34 secs for $a = 0$, and 0.16 to 0.39 secs for $a = 0.95$ (the estimate for a supernova (SN) is 10 sec).

Figure 3 shows the total number of counts in SuperK for these tori as a function of the accretion rate $\dot{M}$. The magenta band corresponds to $a = 0.95$ while the grey one to $a = 0$. The bands for a fixed value of a are obtained by using our two efficiency estimates. The lower limit corresponds to spherical accretion while the upper limit to the spin dependent efficiency. The total events from rapidly accreting tori is larger because these tori are more massive and so there is more material to be converted in neutrino energy. The number of counts can be about an order of magnitude higher for spinning BHs than nonrotating BHs in the case of $\dot{M} = 3M_\odot$. However, this difference is less evident as the accretion rate grows. This is because the efficiency calculated in our first estimate decreases faster with the accretion rate whereas the efficiency in the second estimate is constant for all rates. Therefore the corresponding signal duration for $a = 0$ in the optimistic case will eventually be similar to the pessimistic $a = 0.95$ case. If the accretion rate is low $\sim 3M_\odot/$ sec then we predict a number of counts close to the current SN estimates ($\sim$8000) for a spinning BH and roughly half of the SN events for a nonspinning BH. For higher accretion rates $\sim 9M_\odot/$ sec we could have as much as 4 times the number of events of a SN in the most optimistic scenario.

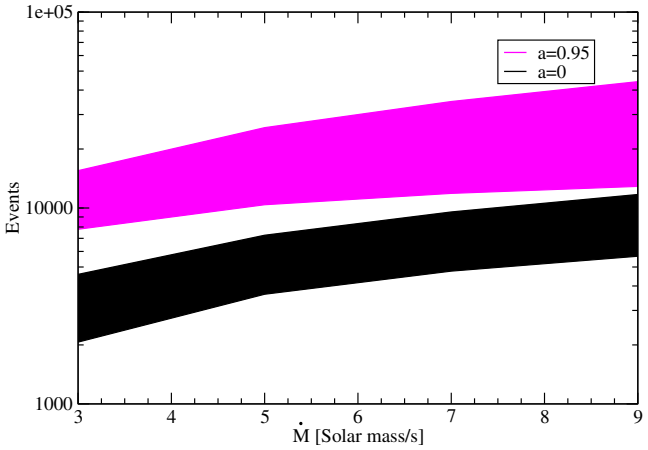

FIG. 3. Total number of events seen at SuperK as a function of mass accretion rate. The tori models are three-dimensional extensions of fully relativistic one-dimensional disks. Indicated is the value of the BH spin. The BH mass is $3M_\odot$ in all the cases.

The predictions for the Just *et al.* model are similar to some extent. As this model is time dependent, we find the accretion mass rate by calculating the total mass of the torus at two different snapshots $t = 20$ ms and $t = 60$ ms so we get $0.146M_\odot/$s. The initial total mass of the torus is $\sim 0.3M_\odot$ [39]. Then $\Delta t = M_T/\dot{M} = 2.05$ sec. With the rates reported in Table I, this implies a total number of counts of $\sim$30, 750 for a BH spin $a = 0$ and $\sim$48, 300 when $a = 0.8$. On the other hand, using an efficiency of $\varepsilon = 0.057$ when $a = 0$ and $\varepsilon = 0.12$ for $a = 0.8$, we find $\Delta t \sim 2.3$ sec for both spin values. This results in a total number of counts of 34,900 and 55,200 for $a = 0$ and $a = 0.8$, respectively. We note that these estimates depend strongly on the duration of the strongest neutrino emission. In reality there will be a period of such intense emission followed by a longer period where the neutrino emission decreases. Some authors estimate for example that this shorter period is on the order of $\sim$50 ms [21]. This timescale predicts event rates on the order of 1000 counts, similar to the grey band in Fig. 3.

V. ANGULAR DEPENDENCE

So far we have considered the detection point to be at 10 kpc on the z axis, perpendicular to the equatorial plane of the axisymmetric torus. However, given the mass distribution of the accreted matter it is natural to expect that neutrino fluxes, rates and any other quantity related to them will change according to the observer's inclination. From one side, the inclination changes the measured solid angle in the observer's sky. Furthermore, neutrinos bend their trajectories due to strong gravity, and regions of the neutrino surface that are invisible in Newtonian gravity could be detected in curved space. On the other hand, some neutrinos that could reach the observer, thanks to the gravitational lensing, can be reabsorbed if on their path to the observer they enter an opaque region. To address these points, we locate the observer at $r_o = 5000$ km away from the BH. This is a reasonable distance that once rescaled to 10 kpc roughly reproduces the rates found above; it is far enough for our treatment of the geodesics in the Schwarzschild metric still to be valid, but close enough to allow us study the effect that the inclination has on the solid angle apparent to the observer. A direct calculation at 10 kpc would be needlessly computationally expensive as the geodesic evaluation over large distances would also require integration steps small enough to achieve impact parameters of the order of km. Rescaling the fluxes at an appropriate distance allows us to study the general relativistic effects on the apparent solid angle Ω_o feasibly and accurately.

We estimate the number of neutrinos observed per unit energy, per unit area, per second as

$$\frac{dN}{dA^o dt^o} = \int dE^o \phi^{\rm eff}(E^o), \tag{20}$$

with the effective flux as in Eq. (16). The observed number of neutrinos per second, luminosities, and average energies are as in Eqs. (5)–(7) but evaluated in the observer's frame (the superscript changed by "o"). In this case, the integral over the area is $4\pi r_o^2$. The integral over the solid angle $d\Omega_o = \sin\xi d\xi d\alpha$ corresponds to the solid angle subtended by the neutrino surface and seen at r_o. The observer is now closer to the BH, and we need to find ξ by explicitly solving the neutrino null geodesics equation. In the Schwarzschild metric, this is

$$\left[\frac{1}{r^2}\left(\frac{dr}{d\varphi}\right)\right]^2 + \frac{1}{r^2}(1 - r_s/r) = \frac{1}{b^2}, \tag{21}$$

where b is, as before, the neutrino's impact parameter, and origin of the spherical coordinates is centered in the BH. The integration of this equation goes from the emission points on the neutrino surface (r_e, φ_e) to the observation point (r_o, φ_o). Once b is found, then ξ (and the solid angle) is given by

$$b = \frac{r_o \sin\xi}{\sqrt{1 - r_s/r_o}}. \tag{22}$$

Neutrinos emitted from a particular point could travel around the BH several times: a neutrino emitted close to the BH can fall into it, reach the exterior with some deflection (first-order image), or rotate around the BH spending more time near the horizon and finally escape to reach the observer (higher-order image). In this study, we limit ourselves to first-order images. Higher orders will also contribute, though the contribution is expected to be subdominant for distant observers and for the BH mass considered here (not the case, however, for massive BHs and closer observers [45,46]).

It is illustrative to compare a Newtonian treatment with the effects that general relativity has on the neutrino fluxes. Figure 4 shows the electron neutrino flux observed on the z axis and at 5000 km from the center of the BH. Here we assume that the disk is optically thick, meaning that only neutrinos emitted from the upper half of the torus reach the observer. The black solid line, labeled as GR, corresponds to the flux when the redshift and bending of the neutrino trajectories are included. The red dashed line (N) shows the fluxes obtained in Newtonian gravity, where the neutrinos travel in straight lines and their energies are not influenced in any way by the BH. In this calculation, neutrinos are emitted anywhere from the torus. We show with the blue dashed-dotted line a calculation where the neutrinos travel in straight lines (no bending), but their energies are redshifted. Finally, with the red dotted line (N_cut) we study a case where the neutrinos fluxes are calculated in Newtonian gravity but we have artificially excluded regions

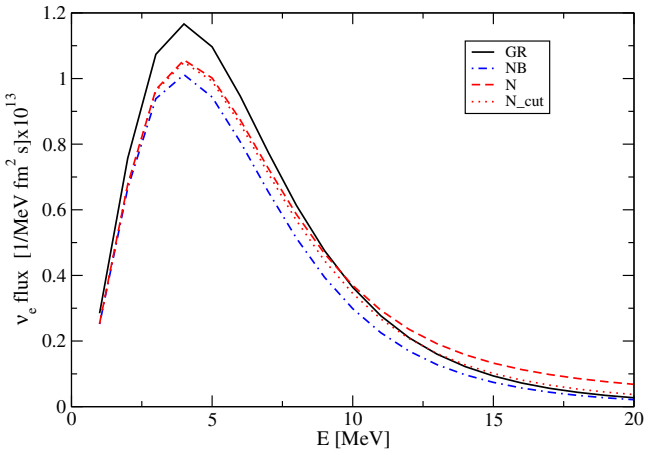

FIG. 4. Electron neutrino fluxes as seen by an observer at 5000 km from a BH of $3M_\odot$, and polar inclination $i = 0°$. The torus model is the steady-state Ca. The black solid line includes all general relativistic effects. The blue dashed-dotted line takes into account redshifts but ignores bending of trajectories. The red dashed line correspond to a Newtonian calculation, while the red dotted line is also Newtonian but assumes that only regions that form first order images in the relativistic case contribute to the fluxes.

of the torus from where emitted neutrinos would had been absorbed by the BH in the GR case.

Compared to a Newtonian treatment, a general relativistic calculation enhances the fluxes at low energies and reduces them in the high energy region. The last fact occurs because high energy neutrinos are emitted from hot regions close to the BH, where the redshift is strong. On the other hand, low energy neutrinos are emitted from regions farther from the BH and their energies are less redshifted. The increased fluxes are a consequence of the larger apparent solid angle derived from the bending of their trajectories. At these larger distances the effect of trajectory bending dominates the redshift. Note also that there is a significant reduction of the fluxes that is caused exclusively by removing neutrinos that could have been absorbed by the BH, as can be seen by comparing the two Newtonian calculations. Although, the $N_{\rm cut}$ calculation also assumes flat space, the fact that removing the neutrino-absorbing regions of the disk brings the fluxes closer to the general relativistic case at high energies (compare dotted and solid lines), highlights the implicit effect of bending of trajectories.

As mentioned above, after neutrinos have left the neutrino surface, they can pass again through an optically thick region on their way to the observer. The apparent solid angle is then not only affected by gravitational lensing but also by neutrino interactions with matter. To study the effect on neutrino fluxes due to changes in the apparent solid angle only, we assume the torus is optically thin. By this we mean that once the neutrinos have decoupled from the optically thick region (at the neutrino surface), they do not reencounter thick regions. In such a case, all the neutrino surface shown in Fig. 5 emits. This provides us with upper limits of our estimates. We contrast these results with two totally thick disks: one as seen by an observer on the z axis (upper half torus, $z > 0$) and one where the observer is located on the $z = 0$ plane, noted by the red dot (not to scale), who will detect the grey surface (roughly half right torus) which starts at the largest distance in the z axis of the neutrino surface; see Fig. 5. For both thick tori, we are assuming that the parts of neutrino surface opposite to the observer are undetected. This will lead to underestimates as neutrinos from those parts can actually reach the observer.

Figure 6 shows the electron neutrino fluxes at 5000 km from the center of the torus. The solid lines correspond to an observer's inclination $i = 0°$, with respect to z axis of the torus, and the dashed lines to $i = 90°$. The thick lines assume the torus is optically thick while the thin lines correspond to an optically thin torus. In this way, an observer located at $i^{\circ} = 0$ will register fluxes that are emitted from the upper half of the neutrino surface only. If the torus is optically thin, neutrinos will reach the observer from the entire neutrino surface (including the lower half). Then at $i = 0°$, the thin fluxes roughly double the thick ones (compare black solid lines). At an inclination of 90° (blue dashed lines), which is on the equatorial plane, the situation is different. If the torus is totally thick, an observer will register fluxes emitted from the grey right half torus in Fig. 5 only, and then the hottest inner parts of the disk will not contribute. In the thin case, neutrinos are emitted everywhere from the neutrino surface, enhancing the fluxes. Furthermore, neutrinos emitted from the opposite half of the neutrino surface can also reach the observer due to strong deflection with lower chances of being reabsorbed (their geodesics do not cross the highest density regions). Additionally, at this angle, the Doppler effect

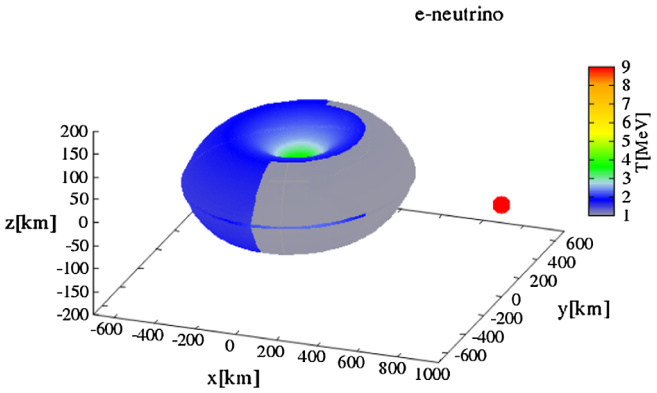

FIG. 5. Electron neutrino surfaces considered in the fluxes calculation shown in Fig. 6. The full torus assumes matter around the disk is neutrino transparent. The upper half of the torus will be detected by an observer in the z axis. The grey right half would be seen by an observer in the $z = 0$ plane (red dot and not to scale) if the torus is opaque. The curved line on the torus shows the intersection of the its surface with the $z = 0$ plane. The torus model is the steady-state Ca with a spin $a = 0.95$ and accretion rate $5M_{\odot}/\mathrm{s}$.

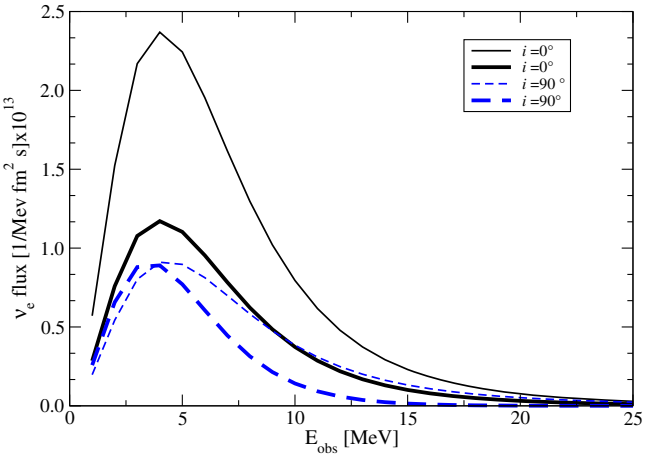

FIG. 6. Electron neutrino fluxes as seen by an observer at 5000 km from a BH of $3M_{\odot}$, and polar inclinations of $i = 0°$ and 90°. The torus model is the steady-state Ca with a spin $a = 0.95$ and accretion rate $5M_{\odot}/\mathrm{s}$. Thin lines correspond to neutrino transparent tori while thick lines to opaque ones.

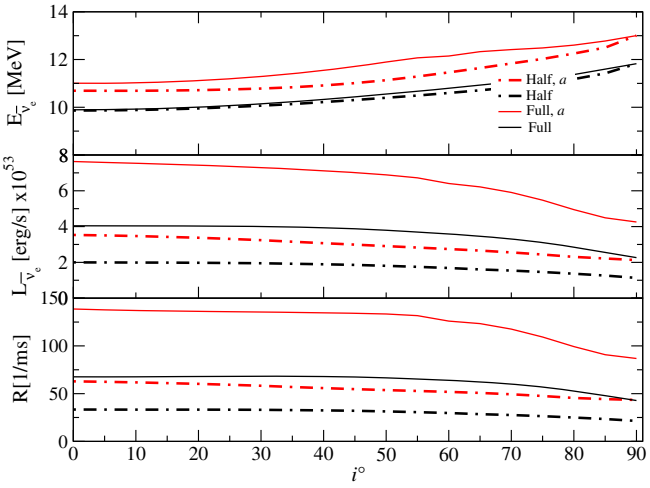

FIG. 7. Electron antineutrino energies, luminosities and detection rates R at SuperK as function of the inclination of the observer with respect to the z axis. The observer is at 5000 km from a BH of $3M_\odot$ and the torus's accretion rate is $5M_\odot/\mathrm{s}$. The rates R are rescaled at 10 kpc. Red and black lines correspond to spins $a = 0.95$ and 0, respectively. Solid lines assume the tori are neutrino transparent while in the calculation showed by the dotted-dashed lines we have used the upper-half of the disk only.

overcompensates the gravitational redshift, due to the angular velocity carried by the disk. The final result are the larger fluxes at higher energies described by the thin blue dashed line.

Based on fluxes obtained at different inclinations, with respect to the z axis, we estimate electron antineutrino average energies, luminosities and detection rates at SuperK. The results are shown in Fig. 7, for a torus of accretion rate $5M_\odot/\mathrm{s}$ and for BH spins $a = 0$ and $a = 0.95$ (C0 and Ca models). The quantities are calculated at 5000 km from the BH and the detection rates have been rescaled to 10 kpc. Red lines correspond to a BH with spin $a = 0.95$ (indicated with a in the legend), while estimates corresponding to a BH with zero spin are represented by black lines. If the torus is neutrino transparent (i.e., assuming they don't reencounter an optically thick region after they leave the neutrino surface), the full neutrino surface is considered and the results are represented by solid thin lines. We contrast these results by considering emission of the upper half only, i.e., above the equatorial plane, of the neutrino surface (dotted-dashed thick lines).

As the inclination increases the solid angle subtended by the neutrino surface decreases, producing a reduction in the luminosities and rates. The average energy, estimated as the ratio between the luminosity and the number of neutrinos per second, becomes insensitive to this reduction. Its behavior is mainly affected by the energy shifts. At zero inclination the neutrino energies observed from different parts of the neutrino surface are all similarly redshifted: gravitational redshift dominates over Doppler shifts. In this case the linear velocity of an element of emitting matter is perpendicular to the observer's. As the inclination increases the linear velocity of the disk becomes parallel to the observer's. Then energies of half the torus are redshifted and the other half appear blueshifted. Thus the shifts in energies are totally different from the shifts in the perpendicular direction. The overall effect is a maximum increase in the observed average energies of about 2 MeV for $a = 0.95$ and 1 MeV for $a = 0$ from $i = 0$ to $i = 90$ deg. Considering a transparent (full) torus has the obvious consequence of having roughly twice the luminosities and rates than the corresponding quantities for a half torus. The small differences in the average energies are due to the fact that the lower parts (for $z < 0$) of the full neutrino surface are farther from the observer who registers different redshifts for neutrinos coming from that area compared to the ones coming from the upper half. When the inclination is 90 degrees the number luminosities and luminosities of the full torus are twice half the disk and the average energies are the same. The differences in average energies when a full or half torus are considered are larger for spinning BHs than for the $a = 0$ case. This is because the energy shift depends on the BH spin and therefore the higher the spin the larger the differences in the average energies between the full and half tori.

VI. SUMMARY AND CONCLUSIONS

Collapsars and BH-NS and NS-NS mergers can evolve into a BH surrounded by an accretion disk. The physics of these objects is crucial in our understanding of gravitational waves, gamma ray bursts and the production of heavy neutron-rich nuclei. The structure of the BH affects the thermodynamic properties of the disk leading to changes in the neutrino surfaces, their fluxes, and consequently in the setting of the neutron to proton fraction, and annihilation rates. We have studied the influence that the BH spin and the location of a distant observer have on several neutrino properties using a ray-tracing technique in general relativity. For the torus model, we have used two different approaches: (1) an extension to three dimensions of a one-dimensional fully relativistic steady state disk and (2) a time-dependent axisymmetric hydrodynamical torus. For both models, we found that the spin of the BH strongly affects the behavior of the neutrino surfaces. Regardless of the flavor, the neutrino surface of an accreting torus around a spinning BH has, when compared to the nonspinning BH, higher neutrino temperatures and larger neutrino surfaces. These characteristics lead to higher neutrino luminosities and average energies. More luminous neutrinos would annihilate at a higher rate and therefore, rotating BHs with total neutrino luminosities $\sim 10^{54}$ are a more likely short gamma ray burst source than steady ones (in agreement with [13]).

Our estimates for neutrino counts per second at SuperK, assuming the source is at 10 kpc, are larger for disks around

spinning BHs, and these detection rates are at least a factor of 10 larger than supernova detection rates, regardless of the torus model. This due to the larger temperatures. The total number of counts and the duration of the signal depend on the efficiency of converting gravitational energy into neutrino energy. Spinning BHs are more efficient and this is reflected in the larger counts we predict compared to the tori around static BHs. For constant accretion rates, we estimate signals lasting tenths of seconds, whereas the number of events varies from few to several thousands (increasing with the accretion rate). For the same disks, we predict that SuperK would be able to detect a neutrino count as far as 0.5 Mpc for an accretion rate of $3M_{\odot}/\mathrm{s}$ in a case of low efficiency and nonspinning BH, and as far as 2 Mpc for the highest accretion rate considered here of $9M_{\odot}/\mathrm{s}$, large efficiency and BH spin $a = 0.95$. Similarly, for the dynamical model of Just *et al.*, we predict that with SuperK we could detect a neutrino as far as ∼2.3 Mpc. In the most pessimistic case, we will observe the Milky Way satellite galaxies and in the most optimistic one we will observe events occurring in Andromeda (∼800 kpc away). The proposed 1 Mton detector Hyper-Kamiokande, with a fiducial volume 560 kton, will detect neutrinos as far as 10 Mpc in the most optimistic scenario.

The fluxes, luminosities, average energies and detection rates depend on the angle that the disk describes in the observer's sky. At larger inclinations the fluxes, luminosities, and detection rates decrease. This is due to the fact that the apparent area of the neutrino surface becomes smaller with increasing angles. Due to Doppler effects, included already in the energy shifts, the average energies increase with the inclination of the observer.

As the possibly observable quantities depend on the apparent emission area to the observer, it is relevant to ask: What is the appropriate neutrino surface for a given observer's inclination? Here we assumed that once the neutrinos decouple from matter, at the last points of scattering, they do not pass through an optically thick region again. This, however, could lead to overestimates, and so we contrast these results with a case where only the upper half of the neutrino surface (on the $z > 0$) emits. For example, in the case of an observer located on the axis perpendicular to the plane of the disk (here z axis), it is reasonable to assume that neutrinos located in the lower half will likely be reabsorbed as they are back to the high density regions "inside" the neutrino surface. Then at zero inclination, our estimates from the upper half of the torus seem reasonable, whereas the full disk provides us with upper limits. However, geodesics coming from the lower part could indeed reach the observer due to the deflection of neutrino trajectories. This effect is stronger as the observer's inclination is increased. For an observer located on the equatorial plane ($i = 90°$) neutrinos emitted from the farthest (opposite) parts of the torus leave the disk with trajectories tangential to the disk and have fewer chances to be reabsorbed. Then gravitational effects would allow us to "see" the opposite side of the neutrino surface. Similarly, the hottest neutrinos emitted near the BH can be strongly deflected and reach the observer contributing to the total flux. At this inclination, considering only a part of the neutrino surface as the emitting area would lead to underestimates. We found that the average energies are not largely affected by these considerations compared to the effects on luminosities and detection rates. The latter could be overestimated by roughly a factor of 2 if the tori are assumed transparent for zero inclination and perhaps by a larger factor for observers near the equatorial plane of the disks. We will leave for future work a detailed study of the effects of reabsorption of the neutrino geodesics.

We expect to take the methodology shown in this work to the next level by working directly with fully relativistic simulations that incorporate neutrino cooling. Initial efforts have already been made in this direction; see e.g. [17,25]. This will allow for a more consistent general relativistic study by solving the Einstein's field equations with neutrino cooling for the matter evolution, and by using ray-tracing in the regions above the neutrino surface for the free-streaming regime. The results presented here also motivate future studies on the effects of the BH spin on the synthesis of elements. Neutrinos set the electron fraction and any changes in the neutrino fluxes will be reflected on the element abundances, particularly in the wind nucleosynthesis [10,47,48]. Furthermore, the properties of the torus outflows will change at different inclinations. The gravitational effects will be much more prominent as the observer, in this case the outflowing matter, is closer to the BH than the observers considered here. We will also address this in future work.

ACKNOWLEDGMENTS

This work was partially supported by the Natural Sciences and Engineering Research Council of Canada (NSERC)(OLC) and by U.S. Department of Energy Grants No. DE-FG02-02ER41216(GCM), No. DE-SC0004786 (GCM), and No. DE-SC0013039(RS).

[1] A. MacFadyen and S. E. Wossley, Astrophys. J. **524**, 262 (1999).
[2] K. Taniguchi, T. W. Baungarte, J. A. Faber, and S. L. Shapiro, Phys. Rev. D **72**, 044008 (2005).
[3] W. H. Lee and W. Kluzniak, Mon. Not. R. Astron. Soc. **308**, 780 (1999).
[4] S. Rosswog, Astrophys. J. **634**,1202 (2005).
[5] J. Abadie *et al.* (LIGO Scientific and VIRGO Collaborations), Classical Quantum Gravity **27**, 173001 (2010).
[6] J. M. Lattimer and D. N. Schramm, Astrophys. J. **192**, L145 (1974).
[7] J. M. Lattimer and D. N. Schramm, Astrophys. J. **210**, 549 (1976).
[8] R. Surman, G. C. McLaughlin, M. Ruffert, H.-T. Janka, and W. R. Hix, Astrophys. J. **679**, L117 (2008).
[9] R. Fernández, D. Kasen, B. D. Metzger, and E. Quataert, Mon. Not. R. Astron. Soc. **446**, 750 (2015).
[10] S. Goriely, A. Bauswein, O. Just, E. Pllumbi, and H. T. Janka, Mon. Not. R. Astron. Soc. **452**, 3894 (2015).
[11] J. Pruet, S. E. Woosley, and R. D. Hoffman, Astrophys. J. **586**, 1254 (2003).
[12] Robert Popham, S. E. Woosley, and Chris Fryer, Astrophys. J. **518**, 356 (1999).
[13] S. Setiawan, M. Ruffert, and H.-Th. Janka, Astron. Astrophys. **458**, 553 (2006).
[14] M. Ruffert and H.-Th. Janka, Astron. Astrophys. **344**, 573 (1999).
[15] K. Nakamura, S. Harikae, T. Kajino, and G. J. Mathews, *Proc. Sci.*, NICXII2012 (2012) 216.
[16] S. Rosswog, Int. J. Mod. Phys. D **24**, 1530012 (2015).
[17] L. Lehner, S. L. Liebling, C. Palenzuela, O. L. Caballero, E. O'Connor, M. Anderson, and D. Neilsen, arXiv: 1603.00501.
[18] S. Nagataki and K. Kohri, Prog. Theor. Phys. **108**, 789 (2002).
[19] G. C. McLaughlin and R. Surman, Phys. Rev. D **75**, 023005 (2007).
[20] O. L. Caballero, G. C. McLaughlin, R. Surman, and R. Surman, Phys. Rev. D **80**, 123004 (2009).
[21] F. Foucart, E. O'Connor, L. Roberts, M. D. Duez, R. Haas, L. E. Kidder, C. D. Ott, H. P. Pfeiffer, M. A. Scheel, and B. Szilagyi, Phys. Rev. D **91**, 124021 (2015).
[22] F. Foucart, M. Brett Deaton, M. D. Duez, E. O'Connor, C. D. Ott, R. Haas, L. E. Kidder, H. P. Pfeiffer, M. A. Scheel, and B. Szilagyi, Phys. Rev. D **90**, 024026 (2014).
[23] M. Brett Deaton, M. D. Duez, F. Foucart, E. O'Connor, C. D. Ott, L. E. Kidder, C. D. Muhlberger, M. A. Scheel, and B. Szilagyi, Astrophys. J. **776**, 47 (2013).
[24] Y. Sekiguchi, K. Kiuchi, K. Kyutoku, and M. Shibata, Phys. Rev. D **91**, 064059 (2015).
[25] C. Palenzuela, S. L. Liebling, D. Neilsen, L. Lehner, O. L. Caballero, E. O'Connor, and M. Anderson, Phys. Rev. D **92**, 044045 (2015).
[26] L. Dessart, C. Ott, A. Burrows, S. Rosswog, and E. Livne, Astrophys. J. **690**, 1681 (2009).
[27] Z. B. Etienne, Y. T. Liu, S. L. Shapiro, and T. W. Baumgarte, Phys. Rev. D **79**, 044024 (2009).
[28] F. Foucart, M. D. Duez, L. E. Kidder, and S. A. Teukolsky, Phys. Rev. D **83**, 024005 (2011).
[29] W.-X. Chen and A. M. Beloborodov, Astrophys. J. **657**, 383 (2007).
[30] I. Zalamea and A. M. Beloborodov, AIP Conf. Proc. **1133**, 121 (2009).
[31] R. Birkl, M. A. Aloy, H.-Th. Janka, and E. Muller, Astron. Astrophys. **463**, 51 (2007).
[32] T. Liu, S. J. Hou, L. Xue, and W. M. Gu, Astrophys. J. Suppl. Ser. **218**, 12 (2015).
[33] S. Harikae, K. Kotake, and T. Takiwaki, Astrophys. J. **713**, 304 (2010).
[34] A. Malkus, J. P. Kneller, G. C. McLaughlin, and R. Surman, Phys. Rev. D **86**, 085015 (2012).
[35] A. Malkus, A. Friedland, and G. C. McLaughlin, arXiv:1403.5797.
[36] R. Surman, O. L. Caballero, G. C. McLaughlin, O. Just, and H. T. Janka, J. Phys. G **41**, 044006 (2014).
[37] O. L. Caballero, G. C. McLaughlin, and R. Surman, Astrophys. J. **745**, 170 (2012).
[38] S. Fukuda *et al.*, Nucl. Instrum. Methods Phys. Res., Sect. A **501**, 418 (2003).
[39] O. Just, A. Bauswein, R. A. Pulpillo, S. Goriely, and H.-T. Janka, Mon. Not. R. Astron. Soc. **448**, 541 (2015).
[40] B. Paczynski and P. Wiita, Astron. Astrophys. **88**, 32 (1980).
[41] I. V. Artemova, G. Bjornsson, and I. D. Novikov, Astrophys. J. **461**, 565 (1996).
[42] O. L. Caballero, G. C. MacLaughlin, and R. Surman, Eur. Phys. J. Web Conf. **93**, 03002 (2015).
[43] A. Perego, S. Rosswog, R. M. Cabezón, O. Korobkin, R. Käppeli, A. Arcones, and M. Liebendörfer, Mon. Not. R. Astron. Soc. **443**, 3134 (2014).
[44] S. L. Shapiro and S. A Teukolsky, *Black Holes, White Dwarfs and Neutron Stars* (Wiley, New York, 1983).
[45] V. Bozza and G. Scarpetta, Phys. Rev. D **76**, 083008 (2007).
[46] K. S. Virbhadra and G. F. R. Ellis, Phys. Rev. D **62**, 084003 (2000).
[47] O. L. Caballero, A. C. Malkus, G. C. McLaughlin, and R. A. Surman, J. Phys. G **41**, 044004 (2014).
[48] D. Martin, A. Perego, A. Arcones, F. K. Thielemann, O. Korobkin, and S. Rosswog, Astrophys. J. **813**, 2 (2015).